



Barnett, W. H., Jenkin, S. E. M., Milsom, W. K., Paton, J., Abdala, A. P., Molkov, Y. I., & Zoccal, D. (2018). The Kölliker-Fuse orchestrates the timing of expiratory abdominal nerve bursting. *Journal of Neurophysiology*, 119(2), 401-412.  
<https://doi.org/10.1152/jn.00499.2017>

Peer reviewed version

License (if available):  
Unspecified

Link to published version (if available):  
[10.1152/jn.00499.2017](https://doi.org/10.1152/jn.00499.2017)

[Link to publication record in Explore Bristol Research](#)  
PDF-document

This is the author accepted manuscript (AAM). The final published version (version of record) is available online via APS at <http://www.physiology.org/doi/10.1152/jn.00499.2017> . Please refer to any applicable terms of use of the publisher.

## University of Bristol - Explore Bristol Research

### General rights

This document is made available in accordance with publisher policies. Please cite only the published version using the reference above. Full terms of use are available:  
<http://www.bristol.ac.uk/red/research-policy/pure/user-guides/ebr-terms/>

**The Kölliker-Fuse orchestrates the timing of expiratory abdominal nerve bursting**

William H. Barnett<sup>1</sup>, Sarah E.M. Jenkin<sup>2</sup>, William K. Milsom<sup>2</sup>, Julian F. R. Paton<sup>3,4</sup>, Ana P. Abdala<sup>\*3</sup>, Yaroslav I. Molkov<sup>\*1,5</sup> and Daniel B. Zoccal<sup>\*6</sup>

<sup>1</sup>Department of Mathematics and Statistics, Georgia State University, Atlanta, GA

<sup>2</sup>Department of Zoology, University of British Columbia, Vancouver, British Columbia, Canada

<sup>3</sup>School of Physiology, Pharmacology and Neuroscience, Biomedical Sciences, University of Bristol, Bristol, United Kingdom

<sup>4</sup>Department of Physiology, Faculty of Medical and Health Sciences, The University of Auckland, Auckland, New Zealand

<sup>5</sup>Neuroscience Institute, Georgia State University, Atlanta, GA

<sup>6</sup>Department of Physiology and Pathology, São Paulo State University, Araraquara, Brazil

\* - joint senior authors

**Running head:** Pontine control of active expiration

**Call for Manuscripts:** Central Pattern Generators

Address for Correspondence:

Daniel B. Zoccal

Department of Physiology and Pathology

School of Dentistry of Araraquara

São Paulo State University (UNESP)

Rua Humaitá, 1680, 14801-903

Araraquara, SP, Brazil

e-mail: zoccal@foar.unesp.br

## New & Noteworthy

- The pons is essential for the formation of the three-phase respiratory pattern, controlling the inspiratory-expiratory phase transition;
- We provide functional evidence of a novel role for the KF controlling the emergence of abdominal expiratory bursts during active expiration;
- A computational model of the respiratory central pattern generator predicts a possible mechanism by which the KF interacts indirectly with the parafacial respiratory group (pFRG) and exerts an inhibitory effect on the expiratory conditional oscillator.

**Keywords:** abdominal expiratory activity, pons, ventral respiratory column, respiratory pattern, active expiration.

**Glossary:** AbN, abdominal nerve; aug-E, augmenting expiratory; BötC, Bötzing complex; CPG, central pattern generator; cVN, vagus nerve; early-I, early-inspiratory; KF Kölliker-Fuse; late-E, late-expiratory; pFRG, parafacial respiratory group; post-I, post-inspiratory; pre-BötC, pre-Bötzing complex; pre-I/I, pre-inspiratory/inspiratory; ramp-I, ramping inspiratory; RTN, retrotrapezoid nucleus;

## ABSTRACT

Coordination of respiratory pump and valve muscle activity is essential for normal breathing. A hallmark respiratory responses to hypercapnia and hypoxia is the emergence of active exhalation, characterized by abdominal muscle pumping during the late one-third of expiration (late-E phase). Late-E abdominal activity during hypercapnia has been attributed to the activation of expiratory neurons located within the parafacial respiratory group (pFRG). However, the mechanisms that control emergence of active exhalation, and its silencing in restful breathing, are not completely understood. We hypothesized that inputs from the Kölliker-Fuse nucleus (KF) control the emergence of late-E activity during hypercapnia. Previously, we reported that reversible inhibition of the KF reduced post-inspiratory (post-I) motor output to laryngeal adductor muscles and brought forward the onset of hypercapnia-induced late-E abdominal activity. Herein, we explored the contribution of the KF for late-E abdominal recruitment during hypercapnia by pharmacologically disinhibiting the KF in *in situ* decerebrate arterially-perfused rat preparations. These data were combined with previous results and incorporated into a computational model of the respiratory central pattern generator. Disinhibition of the KF through local parenchymal microinjections of gabazine (GABA<sub>A</sub> receptor antagonist) prolonged vagal post-I activity and inhibited late-E abdominal output during hypercapnia. *In silico*, we reproduced this behavior and predicted a mechanism where the KF provides excitatory drive to post-I inhibitory neurons, which, in turn, inhibit late-E neurons of the pFRG. Although the exact mechanism proposed by the model requires testing, our data confirm that the KF modulates the formation of late-E abdominal activity during hypercapnia.

## INTRODUCTION

Resting respiratory rhythmogenesis in mammals is suggested to emerge primarily from an inspiratory oscillator located in the medullary respiratory group, which contains neurons that are sufficient to produce rhythmic inspiratory activity *in vitro* (Anderson et al. 2016; Smith et al. 1991). However, generation of the functionally relevant respiratory rhythm and pattern seen *in vivo* requires interactions between the inspiratory oscillator with other respiratory regions (Smith et al. 2007). Accumulating evidence supports the notion that descending inputs from the pontine respiratory group, historically identified as the pneumotaxic center of the brain (Lumsden 1923), are important for generation of eupneic breathing. Within this region, the Kölliker-fuse nucleus (KF) has been identified as an essential region to gate the post-inspiratory (post-I) phase and control I-to-E phase transitions (Dutschmann and Dick 2012; Molkov et al. 2013; Morschel and Dutschmann 2009). The KF contains neurons that provide mainly excitatory synaptic inputs to medullary respiratory regions (Ezure and Tanaka 2006; Geerling et al. 2017; Rosin et al. 2006). Ablation of KF inputs prolongs inspiratory duration and produces apneusis (Bautista and Dutschmann 2014; Harris and Milsom 2003; Molkov et al. 2013; Morrison et al. 1994; St-John and Paton 2004), indicating a significant role of the KF neurons in breathing rhythm generation. Experimental evidence also highlights the role of the KF in the formation of the cranial respiratory motor activity that controls tongue and laryngeal musculature. Microinjection of excitatory amino acid agonists into the KF parenchyma promote tonic excitation of post-I motor activity in the vagus/laryngeal recurrent nerve, increase laryngeal constrictor activity, prolong expiratory phase duration and promote swallowing-related resetting of the respiratory cycle (Abdala et al. 2016; Bonis et al. 2013; Dutschmann and Herbert 2006). In contrast, pharmacological inhibition of the KF eliminates the post-I component of vagus nerve activity, diminishes hypoglossal nerve and genioglossal activities and reduces upper airway resistance (Dutschmann and Herbert 2006; Levitt et al. 2015; Silva et al. 2016a). These studies suggest that KF neurons also interact with the medullary pre-motor respiratory neurons that control upper airway patency during eupnea or oropharyngeal reflexes.

Under conditions of elevated metabolic demand, such as elevated partial pressure of CO<sub>2</sub> (hypercapnia) or low O<sub>2</sub> (hypoxia) in the blood, an active expiratory pattern emerges to support pulmonary hyperventilation (Jenkin and Milsom 2014; Lemes and Zoccal 2014). A distinct feature of active expiration is the generation of rhythmical bursts of abdominal expiratory

activity during the late  $\frac{1}{3}$  of expiration (aka late-E or E2-phase) (Moraes et al. 2014; Pagliardini et al. 2011). In juvenile/adult animals, the generation of abdominal activity relies on the activation of neurons located in the parafacial respiratory group (pFRG), which are suggested to comprise a conditional expiratory oscillator (Abdala et al. 2009; Janczewski and Feldman 2006; Marina et al. 2010; Molkov et al. 2014). Under resting conditions (normoxia and eucapnia), it is suggested that the expiratory pFRG oscillator is synaptically suppressed (de Britto and Moraes 2017; Molkov et al. 2010; Pagliardini et al. 2011; Rubin et al. 2011). During hypercapnia or hypoxia, activation of central and peripheral chemoreceptors brings about rhythmic incrementing bursts in a subpopulation of pFRG neurons, which occur during the late third of the expiratory period (late-E) and correlate with contractions in abdominal expiratory muscles and active exhalation (Abbott et al. 2011; Abdala et al. 2009; Barnett et al. 2017; Marina et al. 2010; Molkov et al. 2011b; Moraes et al. 2012; Silva et al. 2016b). Interestingly, peripheral and central chemoreceptors are suggested to provide tonic excitatory inputs to pontine-medullary respiratory neurons (de Britto and Moraes 2017; Mifflin 1990; Moreira et al. 2007), indicating that synaptic excitatory and inhibitory interactions between the pFRG expiratory oscillator and the respiratory central pattern generator (CPG) are necessary for abdominal pattern formation.

Experiments showing that ponto-medullary transection prevented the emergence of expiratory bursts in abdominal motor nerves during hypercapnia (Abdala et al. 2009) provide evidence for the involvement of the pons in the control of active expiratory motor activity. We recently verified that microinjections of a GABA<sub>A</sub> receptor agonist into the KF parenchyma caused an earlier onset of hypercapnia-induced late-E abdominal activity (Jenkin et al. 2017). These data suggest an inhibitory influence for the KF neurons on the pFRG oscillator, regulating the timing of evoked expiratory bursts in abdominal activity in conditions of metabolic challenge. Although reciprocal connections have been found between the KF and the pFRG regions (Rosin et al. 2006; Silva et al. 2016a), it has been reported that the KF projections to ventromedullary neurons, including those activated during hypercapnia, are predominantly excitatory (Geerling et al. 2017; Yokota et al. 2015) and that local inhibitory neurons are sparse (Abdala et al. 2016; Guthmann et al. 1998). These experimental observations suggest that the inhibitory effect of KF neurons on the pFRG oscillator are indirect.

In light of these observations, in the present study we aimed to further investigate the inhibitory role of KF neurons in the generation of active abdominal expiratory activity.

Specifically, we tested the prediction that artificially increased activity of KF neurons during hypercapnia would cause a suppression of evoked late-E abdominal motor output. The data obtained in this study were combined with our previous experimental findings (Jenkin et al. 2017) were used to extend a previous computational model of the respiratory central pattern generator (CPG) (Molkov et al. 2010; Rybak et al. 2007), then generating a hypothetical model that could provide mechanist insight of how the KF may interact with the respiratory circuitry in the medulla to control late-expiratory abdominal activity during hypercapnia.

## **METHODS**

### ***Experimental data***

Part of the data used here, which relates to pharmacological inhibition of the KF, was extracted from our recently published study (Jenkin et al. 2017) and was re-analyzed in the present paper to be included in the model. The new experimental data presented here were collected as described below.

### **Animals**

The experimental procedures comply with the guidelines of the National Institutes of Health (NIH, publication no. 85-23, 1996) and of the Brazilian National Council for Animal Experimentation Control (CONCEA); and were performed according to the UK Home Office's Animals (Scientific Procedures) Act (1986) and approved by the University of Bristol Animal Welfare and Ethical Review Body. Juvenile male Wistar rats (n=6; P21-25, 50-60 g) were housed with free access to rat chow and water, under controlled conditions of temperature (22 ±1 °C), humidity (50-60%) and light/dark cycle (12:12 lights on at 07:00 am).

### ***In situ* decerebrate arterially perfused rats**

*In situ* decerebrate arterially perfused rats (Paton, 1996) were surgically prepared as previously described (Zoccal et al., 2008). Briefly, rats were heparinized (1000 UI.P.) and subsequently anaesthetized deeply with halothane until the paw and tail pinch reflexes were abolished, transected below the diaphragm and submerged in a cold Ringer solution (in mm: NaCl, 125; NaHCO<sub>3</sub>, 24; KCl, 3.75; CaCl<sub>2</sub>, 2.5; MgSO<sub>4</sub>, 1.25; KH<sub>2</sub>PO<sub>4</sub>, 1.25; dextrose, 10).

They were decerebrated (precollicularly) and the cerebellum was removed to expose the IV ventricle and inferior colliculus. To measure inspiratory motor output, the lungs were removed the left phrenic nerve was cut distally, and recorded using a bipolar suction electrode. To measure motor output to laryngeal abductor and adductor muscles, the left vagus nerve (cVN) was isolated and cut at the cervical level (below the bifurcation of the common carotid artery). To measure output to abdominal muscles, nerves from the right lumbar plexus at thoracic–lumbar level (T12–L1) were dissected and cut distally, and are referred to as abdominal nerve (AbN). Preparations were then transferred to a recording chamber; the descending aorta was cannulated and perfused retrogradely (21–24 mL.min<sup>-1</sup>; Watson-Marlow 502s, Falmouth, Cornwall, UK), via a double-lumen cannula, with Ringer solution containing 1.25% Polyethylene glycol (an oncotic agent, Sigma, St Louis, USA) and vecuronium bromide (a neuromuscular blocker, 3–4 µg.mL<sup>-1</sup>). The perfusion pressure was held within 55–75 mmHg by adding vasopressin (0.5 nM, Sigma, St. Louis, MO, USA) to the perfusate. The perfusate was continuously gassed with 5% CO<sub>2</sub> and 95% O<sub>2</sub> (pH 7.4), warmed to 31–32°C and filtered using a nylon mesh (25 µm). Arterial perfusion pressure was recorded using a Gould transducer and amplifier (Series 6600). Bioelectric signals were amplified (×10,000), band-pass filtered (0.3–5 kHz) (AC Amplifier Model 1700, A-M Systems, Sequim, WA, USA) and recorded using an ADC signal conditioner (10 kHz; Micro1401, Cambridge Electronic Design, Cambridge, UK).

### **Brainstem microinjections**

Microinjections were performed using custom-made, three-barrel glass micropipettes (borosilicate, OD 1.5 mm, ID 0.86 mm, Harvard Apparatus, UK) filled with L-glutamate (10 mM, Sigma-Aldrich, UK), gabazine (a GABA<sub>A</sub> receptor antagonist, 0.1–1 mM, Sigma-Aldrich) and 2% Evans blue dye (Sigma-Aldrich, UK). All drugs were dissolved in artificial cerebrospinal fluid (aCSF) and adjusted to pH 7.4 when needed. The micropipette tips were positioned 0.3–0.5 caudal to the inferior colliculus, 1.9–2.1 mm from the midline and 1–1.5 mm of the dorsal surface, as previously described (Abdala et al. 2016). The location of the microinjections was aided with the use of a surgical binocular microscope and the injection volumes (60 nl) controlled using a pre-calibrated eyepiece reticule. The right and left KF were functionally identified with unilateral glutamate microinjections, which evoked PN burst inhibition and prolonged cVN post-I activity (Dutschmann and Herbert 2006). The left and right-side



identifications were performed in random order, and a time interval of 5 min was allowed between consecutive glutamate microinjections. After a recovery period of at least 10 min, the KF was pharmacologically disinhibited bilaterally through microinjections of gabazine (Mandel and Schreihofer 2009). The contralateral injection of gabazine was always performed within 1-2 min of the first injection. After the experiments, microinjection sites were marked with Evans blue dye and verified histologically *post hoc*. Brainstems were removed and fixed in 4% paraformaldehyde, cryoprotected in 30% sucrose overnight and sectioned in a freezing microtome (40  $\mu$ m). Sections were Nissl counterstained (2% Neutral Red) and mounted with DPX (Sigma-Aldrich, UK). Microinjection sites were photographed and documented on schematic outlines of the dorsolateral pons (Paxinos and Watson 2007).

### **Hypercapnic stimulus**

After stabilization and initial baseline recordings, *in situ* preparations were exposed to hypercapnia by raising the fractional concentration of CO<sub>2</sub> in the perfusate from 5 to 8-10% (balanced with O<sub>2</sub>) for 5 min to generate active expiration (Abdala et al. 2009; Molkov et al. 2011b). The effects peaked and reached steady-state after 3 min of exposure. The stimulus was applied before and after bilateral microinjections of gabazine into the KF.

### **Data analyses**

Analyses were performed on rectified and smoothed signals (time constant of 50 ms) using custom written subroutines in Spike 7.10 software (Cambridge Electronic Design). PN burst frequency was calculated in cycles per minute (cpm). The coefficient of variation (CoV) of PN burst frequency was calculated as an indicator of respiratory cycle variability. The duration of the cVN post-inspiratory component (decrementing activity during the expiratory phase) was expressed as a percentage of total expiratory time (i.e. inter PN burst interval). To quantify AbN activity during eucapnia, each individual expiratory cycle was divided into its initial  $\frac{2}{3}$ , which was dominated by the post-I phase (also known as E1), and the final  $\frac{1}{3}$  which predominantly corresponded to the late-E phase (also known as E2). The maximum amplitudes above baseline of AbN output occurring during the first  $\frac{2}{3}$  and late  $\frac{1}{3}$  of each individual expiratory cycle were measured and averaged over 15-25 cycles (1 min epoch), and expressed in  $\mu$ V. As described previously by Abdala et al. (2009), high amplitude incrementing AbN bursts during the final  $\frac{1}{3}$

of expiration, referred to as AbN late-E bursts, only emerge in conditions of hypercapnia and/or hypoxia, and displayed quantal skyping in relation to PN cycles. To quantify these, a threshold crossing was defined, which was typically set at 75% of the maximum amplitude of AbN activity during the final  $\frac{1}{3}$  of expiration under a hypercapnia challenge. As previously described (Abdala et al. 2009), in order to accommodate it, the occurrence of a high amplitude AbN late-E burst in a given cycle during hypercapnia coincides with a truncated cVN post-I cycle. To quantify this phenomenon during hypercapnia, we subtracted the length of post-I cycles without AbN late-E bursts (non-truncated) from cycles with late-E bursts (truncated), and this is referred to as post-I truncation expressed as  $\Delta PIt$  (ms).

All results are reported as mean  $\pm$  standard errors of the means. The normal distribution of the data was verified using a D'Agostino & Pearson normality test and comparisons were performed using paired nonparametric Wilcoxon t-test. GraphPad Prism (version 6) was used for statistical analyses and differences were considered significant when  $P < 0.05$ .

## **Computational Methods**

The model presented here is an extension of a previous model, which described sensitization of central chemoreceptors (Molkov et al. 2011b). The Molkov et al. (2011b) work drew from Molkov et al. (2010), which investigated the recruitment of the late expiratory oscillator in the pFRG for active expiration. Both models incorporate the network architecture of previous models (Rybak et al. 2007; Smith et al. 2007) inspired by ultra-precise pontine and medullary transection studies. As in our previous models, the respiratory neurons were classified according to their firing pattern (augmenting or decrementing) and phase (inspiratory or expiratory) relative to the phrenic cycle, as recorded experimentally (Abdala et al. 2009; Orem and Trotter 1992; Paton 1996; Rybak et al. 1997): early-inspiratory (early-I); ramping inspiratory (ramp-I); pre-inspiratory (pre-I); post-inspiratory (post-I), augmenting expiratory (aug- E) and late-expiratory (late-E) neurons. Neuronal populations were composed of either 20 or 50 single compartment neuron models described in the Hodgkin-Huxley formalism. Synaptic projections from one population to another were all-to-all, and excitatory projections from drive elements synapsed onto every postsynaptic neuron. The motoneuron output (phrenic nerve, vagus nerve, and abdominal nerve) was computed by integrating the excitatory inputs. The connectivity of this model is detailed in Table 1.

### Distinction from previous models

In contrast to previous models, a hyperpolarization-activated cationic current ( $I_h$ ) was included in the post-I (e) (BötC) population to facilitate adaptation in the post-I component of the cVN motoneuron output. This current followed the Hodgkin-Huxley formalism; its contribution to the current-balance equation was  $I_h = \bar{g}_h m_h (V - E_h)$ , where  $V$  was the membrane potential,  $m_h$  was the activation variable, and the expression  $\bar{g}_h m_h$  determined the instantaneous conductance of the current. The values of its biophysical parameters were adapted from the description in McCormick and Pape (1990). The maximal conductance ( $\bar{g}_h$ ) was 2 nS and the reversal potential ( $E_h$ ) was -43 mV. The activation of  $I_h$  was determined by the equation:

$$\frac{dm_h}{dt} = \frac{f(V) - m_h}{\tau(V)}$$

where the functions for steady state activation  $f(V)$  and time constant  $\tau(V)$  take the following form:

$$f(V) = (1 + \exp([V + 60]/5.5))^{-1} \text{ and} \\ \tau(V) = 1500 / \cosh([V + 80]/13) \text{ ms.}$$

Numerical simulations were performed using NSM 3.0 software, which was developed by S. Markin, I. Rybak, and N. Shevtsova at Drexel University (Rybak et al. 2007; Rybak et al. 2004). It was extended to use OpenMPI for high-performance computing clusters by Y. Molkov (Molkov et al. 2011b). Solutions to ordinary differential equations were computed using the exponential Euler method for integration with a time step of 0.1 ms.

### Model adjustments

The response to hypercapnia in the model is mediated by an increase in a tonic drive attributed to chemosensitive neurons in the RTN. The targets of this drive are the pFRG late-E population and the pre-I/I population of the pre-BötC. The latter population, in turn, could also excite late-E populations in the pFRG and contribute to the generation of late-E activity (Barnett et al. 2017). The gain of this drive with changing CO<sub>2</sub> was set to support late expiratory activity in the late-E population of the pFRG. We also considered that, for pattern formation, pFRG late-E neurons receive phasic inhibition during early-inspiration and post-inspiration from the

respiratory CPG (Abdala et al. 2009; Molkov et al. 2010; Rubin et al. 2011), which in turn is excited by a tonic drive from the pons (Rybak et al. 2007; Smith et al. 2007).

Anatomical (Gang et al. 1995) and electrophysiological studies (Ezure and Tanaka 2006) indicate the existence of synaptic projections from the KF to the BötC region. Based on these observations, and on studies showing that the majority of projections from the KF to lower brainstem respiratory groups are glutamatergic (Geerling et al. 2017), we proposed that an inhibitory post-I population of BötC neurons are under direct control by a KF population, which we model as a tonic excitatory drive (highlighted in Figure 5). Under eupneic conditions, the KF-driven post-I population of the BötC inhibits both the RTN/pFRG expiratory population and the pre-I/I population. This inhibition suppresses late expiratory activity in the RTN/pFRG and contributes to the timing of the onset of inspiration (Figure 5). Our data (this study and Jenkin et al., 2017) demonstrate that mild inhibition and disinhibition of the KF nucleus modulates the emergence of late-E activity during hypercapnia, without significantly disrupting eucapnic respiration. Thus, we reasoned that drive from the KF should also be distributed among both inspiratory and expiratory populations (Figure 5), and inhibition or disinhibition of the KF nucleus should result in relatively balanced changes in drive to inspiratory and expiratory populations of the respiratory central pattern generator. In previous iterations of the model (Barnett et al. 2017; Molkov et al. 2010), a component of the tonic drive to the early-I population of the pre-BötC was attributed to the pontine nuclei. Therefore, in the model of the present study, we attributed a portion of the pontine drive received by the early-I population of the pre-BötC to the KF (highlighted in Figure 5). For the purposes of simulation, inhibition of the KF was interpreted as a decrease in the excitatory drive by 35%, and disinhibition of the KF was interpreted as an increase in the excitatory drive by 30%. These percentage changes in excitatory conductance of the neurons receiving the KF drive were the values that best reproduced our experimental data. The remaining pontine drive was separate and independent from the KF drive and was invariant during increases or decreases to the KF drive.

We also adjusted network topology to promote pre-inspiratory and late-E activity that is distinct in time from inspiratory activity. In Molkov et al. (2010) and Molkov et al. (2011b), the late-E pFRG population stimulated the pre-I/I population. This projection promoted entrainment of pre-I/I activity to the pFRG expiratory oscillator. In Barnett et al. (2017), an excitatory projection from the pre-I/I population to the late-E (pFRG) population was included so that an

increased excitability of the pre-I/I population could lower the threshold for emergence of late-expiratory activity. Here, we removed the excitatory projection from the late-E (pFRG) population to the pre-I/I population. Excitation from the pre-I/I to the early-I population of the pre-BötC was diminished, and a component of the phasic excitation to the early-I population was replaced by a tonic drive, which is sufficient to support an inspiratory burst at the termination of expiration. We also incorporated an excitatory projection from the late-E pFRG expiratory population into the respiratory CPG that excited the augmenting expiratory (aug-E) population of the BötC. In the event of a burst in the RTN/pFRG expiratory oscillator, increased input to aug-E serves to prevent inspiratory burst initiation during the late-E burst in the pFRG, in agreement with previous experimental observations (Abdala et al. 2009).

## RESULTS

### Anatomical and functional identification of microinjections sites in the KF

Unilateral microinjections of glutamate in the KF increased post-I activity in the cVN, prolonged expiratory time and reduced PN burst frequency, as illustrated in Figure 1A. Stimulation of the KF with glutamate did not alter the magnitude of resting AbN activity (Figure 1A). *Post-hoc* histological analyses confirmed that the microinjection sites were in the boundaries of the KF (Figure 1B), between -8.64 and -8.88 mm in relation to Bregma (Figure 1C) (Paxinos and Watson 2007).

### Baseline respiratory changes after disinhibition of the KF

Under resting conditions (eucapnia), the PN burst showed a ramping pattern of discharge, the cVN presented an inspiratory component (coincident with the PN burst) followed by post-I decrementing activity, and the AbN exhibited low-amplitude activity (relative to hypercapnia) during the expiratory phase, which was typically decrementing during the first  $\frac{2}{3}$  of expiration. One preparation also had low amplitude incrementing AbN activity during the final  $\frac{1}{3}$  of expiration. Bilateral microinjections of low doses of gabazine in the KF caused a small but significant increase in the duration of post-I activity in the cVN ( $68 \pm 7$  vs  $59 \pm 6$  % of expiratory time,  $P < 0.05$ , Figure 2A, B). This effect was accompanied by an increase in PN burst frequency variability (CoV:  $0.36 \pm 0.10$  vs  $0.15 \pm 0.04$ ,  $P < 0.05$ , Figure 2C), with no changes in: PN burst frequency ( $23 \pm 4$  vs  $21 \pm 4$  cpm, Figure 2D), time of inspiration ( $0.662 \pm 0.05$  vs  $0.757 \pm 0.085$  s)

and time of expiration ( $2.72 \pm 0.41$  vs  $2.96 \pm 1.02$  s). Baseline mean AbN activity ( $3.81 \pm 0.72$  vs  $3.96 \pm 0.71$   $\mu$ V, Figure 2E) did not change after gabazine microinjections in the KF.

### **Effect of disinhibition of the KF on the generation of late-E bursts during hypercapnia**

With the increase in the fractional concentration of CO<sub>2</sub> in the perfusate (8-10%), late-E bursts emerged in AbN activity (Figure 3) at a relative frequency ratio of 1:2 with the PN burst (Figure 3A-C) and 1:1 ratio with the PN frequency at 10% CO<sub>2</sub> (Figure 3D-E). Concomitantly, post-I duration in the cVN was reduced significantly (Figure 4A and 4D). No significant changes were observed in PN frequency during steady-state hypercapnia. After disinhibition of the KF, the magnitude of the AbN late-E response to hypercapnia was markedly suppressed (Figure 3F-H, Figure 4B) ( $\Delta$ :  $8.2 \pm 0.7$  vs  $1.8 \pm 0.9$   $\mu$ V, respectively before and after gabazine,  $P < 0.05$ ; Figure 4C). This lower amplitude of AbN late-E bursts after gabazine microinjections was associated with a reduced cVN post-I truncation ( $\Delta$ PIt:  $-0.276 \pm 0.070$  vs  $-0.137 \pm 0.069$  s, respectively before and after gabazine microinjections,  $P < 0.05$ , Figure 4D). No significant changes were noted in the PN frequency during steady-state hypercapnia before versus after gabazine microinjections in the KF ( $\Delta$ :  $2 \pm 1$  vs  $4 \pm 2$  cpm, respectively). Sixty minutes after gabazine microinjections, the magnitude of late-E bursts in AbN ( $\Delta$ :  $5.5 \pm 0.6$   $\mu$ V) and the cVN post-I truncation ( $\Delta$ PIt:  $-0.551 \pm 0.147$  s) evoked by hypercapnia were equivalent to pre-treatment values.

### **Proposed mechanisms through model adjustments**

We performed a series of computational experiments aimed at proposing a model that explains the changes to late-E activity in the AbN pattern during active expiration obtained in both this study as well as in our previous related study (Jenkin et al. 2017). Based on the sum of the data, we identified the following key features of the motoneuron output during hypercapnia after pharmacological manipulation of the KF: (1) microinjections of isoguvacine (GABA<sub>A</sub> receptor agonist) to inhibit the KF during hypercapnia suppressed the post-I component of the cVN and advanced the onset of late-E activity in the AbN, increasing its burst duration (Jenkin et al. 2017); (2) disinhibition of the KF during hypercapnia attenuated the shortening in post-I activity of cVN and reduced AbN late-E activity (present study). Our model was adjusted to reproduce these findings, as described in the Methods section (*Model adjustments*).

## Model validation

### *Transient activation of KF drive in the model induces apnea.*

Application of glutamate in the KF evokes respiratory apnea during which there is increased post-I activity in the vagus nerve (Figure 2). We reproduced these results by transiently increasing the KF drive by a factor of 4 (Figure 6). Post-I (BötC) activity increased in amplitude and became tonic for the duration of the stimulation period; this population strongly inhibited aug-E (BötC) neuron activity. The excitatory pre-motor post-I (e) (BötC) population is responsible for the post-inspiratory component of cVN, and it receives strong inhibition from aug-E (BötC) neurons. During the epoch of increased drive from the KF, post-I (e) (BötC) activity was disinhibited since aug-E (BötC) neurons did not fire, hence the activity in the cVN persisted for the duration of the excess KF input.

### *Suppression of KF drive enhances inspiratory phase duration.*

Previous studies have reported that inhibition of KF neurons reduces post-inspiratory vagal activity and enhances inspiratory phase duration, but does not modify baseline abdominal activity (Bautista and Dutschmann 2014; 2016; Jenkin et al. 2017). Our model simulations, which compared the activity of pre-BötC, BötC and pFRG populations in eucapnia before (Figure 7A) and after KF inhibition (Figure 7B), agree with these previous experimental observations. KF inhibition in eucapnia reduced the overall firing rate of the post-I (BötC) populations (inhibitory and excitatory) and increased the phase duration and firing frequency of the pre-I/I (pre-BötC) population (Figure 7B) compared to the control simulation (Figure 7A). Also, KF inhibition did not modify the activity of the late-E (pFRG) population.

### *The role of KF drive and pre-I excitation in active expiration*

In our previous models, the emergence of active expiration during hypercapnia was dependent on an increase in the chemosensory drive from the RTN (Molkov et al. 2010; Molkov et al. 2011b). The same mechanism was implemented in this model. However, the late-E (pFRG) population also received increased excitatory input from the pre-I/I (pre-BötC) population during the E2 phase. To investigate the role of pre-I/I (pre-BötC) activity in the emergence and modulation of active expiration, we performed simulations in eucapnia (control simulation; Figure 7A) and eucapnia with KF inhibition (Figure 7B). KF inhibition in eucapnia reduced the

overall firing rate of the post-I (BötC) population and increased the phase duration and firing frequency of the pre-I/I (pre-BötC) population (Figure 7B) compared to the control simulation (Figure 7A). Pharmacological disinhibition of the RTN/pFRG was shown to be sufficient to evoke late-E activity (Molkov et al. 2010; Pagliardini et al. 2011). However, in Jenkin et al. (2017), application of isoguvacine to the KF during eucapnia failed to evoke active expiration. Consistently, in these modeling results, reduction of the KF drive to post-I (BötC) populations created a combination of weak expiratory disinhibition and weak expiratory excitation, which was not sufficient to evoke late-E activity in accordance with the isoguvacine experiments during eucapnia.

## **Model performance**

### *Suppression of the KF drive increases AbN late-E burst duration by reducing post-I inhibition*

We implemented a pharmacological inhibition of the KF with isoguvacine in our extended model to explain the change in motoneuron output observed in our previous experimental results (Jenkin et al. 2017). This was simulated by a decrease in the tonic KF drive to the post-I (BötC) and early-I (pre-BötC) populations, and we refer to this manipulation in simulation as inhibition of the KF. Our analysis also included a simulation of hypercapnia with reduced KF drive (motoneuron output in Figure 8A; central pattern generator activity in Figure 9A) and a simulation of the control condition – hypercapnia only (motoneuron output in Figure 8B; central pattern generator activity in Figure 9B). Similar to the rat experiments with isoguvacine, a partial decrease in the KF drive during hypercapnia did not disrupt the three-phase respiratory rhythm in the model. Also, the model reproduced the advanced onset and increased phase duration of the AbN late-E burst in hypercapnia with reduced KF drive (Figure 8A) as compared to hypercapnia with no additional manipulation to the KF (Figure 8B).

In this model, the post-I (BötC) population fires in a decrementing fashion through the duration of expiration (Figure 9) and is a main source of expiratory inhibition in the respiratory cycle. The late-E (pFRG) population receives both expiratory and inspiratory inhibition in eucapnia (Figure 5). During hypercapnia, the increase in tonic chemosensitive drive from the RTN lowers its threshold for activation. As the firing rate of the post-I (BötC) population decrements to a critical value, inhibition of late-E (pFRG) neurons decreases such that the population fires at the end of expiration (Figure 9B). In the simulation including both reduced



KF drive and hypercapnia, the average firing rate of post-I (BötC) neurons is reduced. As such, late-E (pFRG) neurons reach their threshold for activation earlier in the expiratory phase (Figure 9A) and the duration of late-E bursts extends over a longer interval at the end of expiration.

In Jenkin et al. (2017), inhibition of the KF during hypercapnia decreased the amplitude of post-I activity in the cVN. In the current model, the excitatory post-I (e) (BötC) population shapes the post-inspiratory component of the cVN activity (Figure 5). This population receives strong inhibition from aug-E neurons (BötC); this inhibition determines the phase duration of post-I (e) (BötC) activity and, hence, the phase duration of the post-inspiratory component of cVN activity. The onset time of aug-E activity (BötC) in the respiratory cycle is determined by the inhibition that it receives from the inhibitory post-I neurons (BötC). This inhibition is gradually removed as post-I activity decrements and aug-E activity is eventually released. In the simulation of hypercapnia and KF inhibition, the average firing rate of post-I neurons (BötC) is decreased and aug-E (BötC) activity is recruited earlier in the expiratory phase (Figure 9A; Figure 10) compared to the hypercapnia simulation (Figure 9B; Figure 10). In this way, the phase duration of post-I (e) (BötC) and the post-inspiratory component of the cVN activity is reduced through disinhibition of aug-E neurons.

#### *Amplification of post-I inhibition abolishes AbN late-E activity.*

The effect of microinjections of gabazine in the KF was reproduced in the current extended model by increasing the KF drive to post-I (BötC) and early-I (BötC) neurons, and we refer to this manipulation as disinhibition of the KF. It is important to note that our model simulations reproduced the effects caused by the doses of gabazine used in the present experimental study, which did not disrupt the three-phase breathing pattern and differ from results of another study that used higher concentrations of GABA<sub>A</sub> receptor antagonists (Abdala et al. 2016). The simulation of hypercapnia and KF disinhibition (Figure 8C; Figure 9C) compliments the simulation of hypercapnia and KF inhibition (Figure 8A; Figure 9A) and the simulation of hypercapnia alone (control condition; Figure 8B; Figure 9B). In our simulations, the model reproduced the suppression in the AbN motoneuron output after KF disinhibition (Figure 8C). We attributed the suppression of active expiration to the increase in the tonic KF drive to the inhibitory post-I neurons (BötC). The average firing rate of the post-I (BötC) population increased during simulation of hypercapnia and disinhibition of the KF (Figure 9C)

compared to the simulation of hypercapnia without perturbation to the KF drive (Figure 9B). The increase in firing rate of the post-I population (BötC) lead to an overall increase in inhibition of late-E neurons (pFRG) during expiration such that late-E activity (pFRG) could not be activated despite increased chemosensitive drive from the RTN.

The post-I (e) (BötC) population increased its firing duration (Figure 9C). An increase in average firing rate of the post-I (BötC) population distributed more inhibition to its post-synaptic targets. This increase in inhibition is offset in the early-I population by the increase in tonic KF drive, but there is no mechanism to compensate for the increase in inhibition to aug-E (BötC) neurons. The onset time of the E2 burst of aug-E (BötC) neurons was delayed, and, thus, the duration of post-I (e) (BötC) activity increased (Figure 9C; Figure 10).

## DISCUSSION

Active expiration emerges as a reflex mechanism to increase minute ventilation and support blood gas homeostasis in states of high metabolic demand (Jenkin and Milsom 2014; Lemes and Zoccal 2014). An important motor component of the active expiratory pattern is the development of high-amplitude bursts in abdominal expiratory motor activity, not seen in eupnea. Under hypercapnic conditions, these abdominal bursts are present during the late-E phase of the respiratory cycle, in association with reduced upper airway resistance and increased sympathetic outflow (Abdala et al. 2009; de Britto and Moraes 2017; Molkov et al. 2011a). This evoked late-E discharge in AbN activity reported in the decerebrate *in situ* preparation resembles the pattern recorded in *in vivo* (more intact) preparations (Iizuka and Fregosi 2007; Moraes et al. 2013; Pagliardini et al. 2011), indicating that this pattern formation depends primarily on neural mechanisms within the brainstem. In the present study, we provide novel insights supporting a conditional inhibitory role of the KF neurons regulating the timing of abdominal late-E bursts in conditions of high chemosensory drive. Based on experimental data, we present modeling simulations elucidating possible interactions between the KF and the pFRG, through the BötC, which might help to explain, at least in part, the inhibitory effect of KF inputs on the threshold for activation of the expiratory oscillator.

The generation of active expiration has been attributed to a conditional expiratory oscillator located in the pFRG (Janczewski and Feldman 2006), whose activity is suggested to be defined by a balance between excitatory and inhibitory inputs (Marina et al. 2010; Molkov et al.

2010; Moraes et al. 2012; Pagliardini et al. 2011; Rubin et al. 2011). Under normoxic/eucapnic conditions, the expiratory neurons of the pFRG are tonically suppressed by inhibitory synapses (Pagliardini et al. 2011). During hypercapnia or hypoxia, this oscillator is activated due to increased excitation from central and peripheral chemoreceptors (Marina et al. 2010; Moraes et al. 2012) and reduction in the inhibitory drive to the pFRG (Abdala et al. 2009; de Britto and Moraes 2017). Under eucapnic normoxic conditions, activation and disinhibition of the KF with microinjections of glutamate and gabazine, respectively, did not modify abdominal activity. This finding agrees with previous studies demonstrating that baseline abdominal activity did not change after inhibition of the KF, despite significant modifications in phrenic and vagal motor outputs (Bautista and Dutschmann 2016; Jenkin et al. 2017). These data suggest that, under resting conditions, the KF inputs to the respiratory CPG are important for three-phase respiratory pattern formation, contributing to the inspiratory off-switch and the control of inspiratory-expiratory phase transition (Dutschmann et al. 2014), but do not influence the generation of abdominal activity and the activity of pFRG expiratory neurons.

On the other hand, pharmacological manipulations of the KF during hypercapnia revealed that changes in KF drive to the respiratory CPG affect the emergence and timing of the AbN late-E activity in conditions of elevated chemosensitive drive. We previously demonstrated in rats that inhibition of the KF with isoguvacine reduced baseline post-I vagal activity and advanced the onset of late-E abdominal bursts in the expiratory phase (Jenkin et al. 2017). Herein, we report that KF disinhibition with low doses of gabazine (100  $\mu$ M) during hypercapnia generate a modest increase in baseline post-I activity in the vagus nerve, but markedly attenuate the emergence of late-E bursts in the abdominal motor output. In these experiments, we sought to promote a moderate disinhibition of the KF by using lower doses of a GABA<sub>A</sub> receptor antagonist [100  $\mu$ M of gabazine versus 5 mM of bicuculline in Abdala et al. (2016)] to avoid excessive KF overactivity and the generation of exaggerated post-I bursts in vagus nerve activity associated with periods of apnea, as described previously (Abdala et al. 2016). These findings reveal a conditional inhibitory role of the KF that effectively controls the timing and generation of abdominal bursts during hypercapnia. Teppema et al. (1997) reported an increase in fos expression at the region of the KF after hypercapnia exposure. Interestingly, most of hypercapnia-activated KF neurons that send projections to respiratory neurons in the lower brainstem and spinal cord are glutamatergic (Yokota et al. 2015). Based on this, we hypothesize

that the KF impedes the emergence of late expiratory activity through an indirect inhibitory pathway that controls the pFRG neuronal activity. The recruitment of this KF-driven pathway during hypercapnia might be important for promoting phasic inhibition of expiratory neurons in the pFRG, then contributing to late-expiratory pattern formation. Interestingly, modifications in the strength of this pathway may modulate the active expiratory pattern, as seen during sleep-wake cycles (Andrews and Pagliardini 2015; Leirao et al. 2017).

We consider the possibility that the KF controls the threshold for activation of the late-E (pFRG) neuronal population and the emergence of late-E activity in the AbN through inhibition from post-I (BötC) neurons. This assumption was based on the following experimental observations: i) projections from the KF to the other pontine and medullary regions that control respiratory function are predominantly excitatory (glutamatergic) (Geerling et al. (2017); ii) we found an inverse relationship between post-I and late-E motor activities (present study and Jenkin et al., 2017); iii) post-I neurons of the BötC are suggested as an important source of inhibition to the pFRG (Molkov et al. 2010); iv) the activity of post-I neurons in the BötC requires pontine drive (Smith et al., 2007); and v) studies using retrograde labeling (Gang et al. 1995) and antidromic stimulation (Ezure and Tanaka 2006) suggest the existence of projections from the KF to the BötC region. This hypothesis was incorporated and tested in our model of respiratory CPG. In this model, the KF provided an excitatory drive to inhibitory post-I neurons in the BötC, which, in turn, inhibited late-E neurons in the pFRG. This KF-driven post-I population in the BötC also established inhibitory connections with inspiratory population in the pre-BötC. In model simulations, mild KF inhibition during hypercapnia led to suppression of post-I (BötC) activity which reduced the threshold necessary for the activation of late-E (pFRG) neurons, thus advancing the breakthrough of late-E activity and prolonging its burst duration. In the simulation of mild KF disinhibition during hypercapnia, the enhanced post-I (BötC) activity did not decrement enough to release late-E (pFRG) activity. Hence, late-E bursts did not appear in the AbN. Therefore, our modeling simulations suggest a potential mechanism by which KF inputs may determine the intensity of post-I (BötC) discharge, which, in turn, finely controls the emergence of AbN late-E activity and its duration during hypercapnia. This theoretical mechanism still awaits experimental confirmation but parallels previous studies showing that more extreme reductions in the pontine drive to post-I (BötC) neurons, as seen in conditions of

ischemia, generate late-E/post-I biphasic abdominal bursts (Abdala et al. 2009; Molkov et al. 2010; Rubin et al. 2011).

Previously, we investigated the role of phasic ponto-medullary interactions in models that included pulmonary feedback (Molkov et al. 2013; Rybak et al. 2004). Based on these interactions, it is safe to assume that, qualitatively, the variation of excitability of pontine neurons would give rise to variation in the tonic drive to the populations they project to. Therefore, in the present study, for simplicity, we implemented the contributions of the pontine nuclei as a variable tonic excitatory drive. This allowed us to make some generic assumptions about the effect of the pharmacological manipulations delivered by isoguvacine and gabazine without addressing specific cell-types in the pons. Those assumptions were: (1) there is a tonic pontine drive that is invariant in the face of these manipulations: and (2) there is a tonic pontine drive that we attribute to the KF whose amplitude is subject to our manipulations. This simplification also allowed us to formulate a specific hypothesis for the role of KF input to the CPG in the regulation of the emergence of active expiration.

Previous studies demonstrated that the antagonism of GABA<sub>A</sub> and glycinergic receptors in the pFRG generates abdominal late-E activity under normoxic and eucapnic conditions (de Britto and Moraes 2017; Molkov et al. 2010; Pagliardini et al. 2011). Our current model supports the hypothesis that late-E activity is markedly controlled by inhibitory inputs from the respiratory CPG. In our *in situ* experiments, we observed that KF inhibition did not evoke active expiration at rest (Jenkin et al. 2017). Although our microinjections may have not inhibited all neurons in the KF, these data suggest that other sources of inhibitory input to the pFRG may also contribute to tonic inhibition of the expiratory oscillator. These sources may include inhibitory projections from the nucleus of the Solitary Tract (NTS) (Takakura et al. 2007).

In conclusion, our experimental data indicate that KF-driven inputs to the respiratory CPG control the presence and onset timing of AbN late-E bursts during exposure to high CO<sub>2</sub>. Our model simulations propose that this inhibitory effect of the KF on hypercapnia-induced AbN activity is indirect and involves connections with post-I neurons of the BötC, which, in turn, inhibit expiratory neurons in the pFRG. Although the proposed model requires further anatomic and functional validation, our findings are relevant for exploring the mechanisms underpinning the generation of active expiration in conditions of chronic intermittent (Zoccal et al. 2009; Zoccal et al. 2008) or sustained hypoxia (Moraes et al. 2014). In these experimental conditions,

the emergence of late-E activity at rest is suggested to be associated with depressed post-I BötC activity (Moraes et al. 2014; Zoccal et al. 2008) and sensitization of chemosensitive neurons in the RTN (Molkov et al. 2011a). Therefore, the hypoxia-induced reduction of the pontine drive to the medullary respiratory circuits, causing a reduction in excitability of the post-I (BötC) population, may promote active expiration in eucapnia by reducing the baseline expiratory inhibition in late-E. Moreover, hyperactivity of the KF neurons has been suggested as a mechanism that generates respiratory instabilities in the mouse model of Rett syndrome (Abdala et al. 2016). During central apneas in *Mecp2*-deficient mice, sustained expiratory activities are observed in the hypoglossal, vagus and abdominal nerves (Abdala et al. 2010). This mouse model also exhibits reduced ventilatory responses to hypercapnia (Toward et al. 2013). Although our current model does not explain the generation of the respiratory phenotype seen in Rett Syndrome, it certainly forms a platform from which to conceptualize the mechanisms responsible for the generation of central apneas and respiratory cycle irregularity in multiple disorders.

## GRANTS

This study was supported by NIH (grant R01AT008632), NIH (grant U01 EB21960) and São Paulo Research Foundation (FAPESP, grant 2013/17.251-6). This work utilized the computational resources of the NIH HPC Biowulf cluster (<http://hpc.nih.gov>).

## DISCLOSURES

No conflicts of interest are declared by the authors.

## AUTHOR CONTRIBUTION

APA and DBZ conceived and designed the experiments. DBZ performed all the *in situ* experiments. WHB and YIM designed and performed modeling simulations. APA, DBZ, WHB and YIM assembled, analyzed and interpreted the data. DBZ, WHB and YIM drafted the article. APA, DBZ, JFRP, SEMJ, WHB, WKM and YIM revised and edited the article critically for important intellectual content. All authors have approved the final version of the manuscript.

## REFERENCES

- Abbott SB, Stornetta RL, Coates MB, and Guyenet PG.** Phox2b-expressing neurons of the parafacial region regulate breathing rate, inspiration, and expiration in conscious rats. *J Neurosci* 31: 16410-16422, 2011.
- Abdala AP, Dutschmann M, Bissonnette JM, and Paton JF.** Correction of respiratory disorders in a mouse model of Rett syndrome. *Proc Natl Acad Sci U S A* 107: 18208-18213, 2010.
- Abdala AP, Rybak IA, Smith JC, and Paton JF.** Abdominal expiratory activity in the rat brainstem-spinal cord in situ: patterns, origins and implications for respiratory rhythm generation. *J Physiol* 587: 3539-3559, 2009.
- Abdala AP, Toward MA, Dutschmann M, Bissonnette JM, and Paton JF.** Deficiency of GABAergic synaptic inhibition in the Kolliker-Fuse area underlies respiratory dysrhythmia in a mouse model of Rett syndrome. *J Physiol* 594: 223-237, 2016.
- Anderson TM, Garcia AJ, 3rd, Baertsch NA, Pollak J, Bloom JC, Wei AD, Rai KG, and Ramirez JM.** A novel excitatory network for the control of breathing. *Nature* 536: 76-80, 2016.
- Andrews CG, and Pagliardini S.** Expiratory activation of abdominal muscle is associated with improved respiratory stability and an increase in minute ventilation in REM epochs of adult rats. *J Appl Physiol (1985)* 119: 968-974, 2015.
- Barnett WH, Abdala AP, Paton JF, Rybak IA, Zoccal DB, and Molkov YI.** Chemoreception and neuroplasticity in respiratory circuits. *Exp Neurol* 287: 153-164, 2017.
- Bautista TG, and Dutschmann M.** Inhibition of the pontine Kolliker-Fuse nucleus abolishes eupneic inspiratory hypoglossal motor discharge in rat. *Neuroscience* 267: 22-29, 2014.
- Bautista TG, and Dutschmann M.** The role of the Kolliker-Fuse nuclei in the determination of abdominal motor output in a perfused brainstem preparation of juvenile rat. *Respir Physiol Neurobiol* 226: 102-109, 2016.
- Bonis JM, Neumueller SE, Krause KL, Pan LG, Hodges MR, and Forster HV.** Contributions of the Kolliker-Fuse nucleus to coordination of breathing and swallowing. *Respir Physiol Neurobiol* 189: 10-21, 2013.
- de Britto AA, and Moraes DJ.** Non-chemosensitive parafacial neurons simultaneously regulate active expiration and airway patency under hypercapnia in rats. *J Physiol* 595: 2043-2064, 2017.
- Dutschmann M, and Dick TE.** Pontine mechanisms of respiratory control. *Compr Physiol* 2: 2443-2469, 2012.
- Dutschmann M, and Herbert H.** The Kolliker-Fuse nucleus gates the postinspiratory phase of the respiratory cycle to control inspiratory off-switch and upper airway resistance in rat. *The European journal of neuroscience* 24: 1071-1084, 2006.
- Dutschmann M, Jones SE, Subramanian HH, Stanic D, and Bautista TG.** The physiological significance of postinspiration in respiratory control. *Prog Brain Res* 212: 113-130, 2014.
- Ezure K, and Tanaka I.** Distribution and medullary projection of respiratory neurons in the dorsolateral pons of the rat. *Neuroscience* 141: 1011-1023, 2006.
- Gang S, Sato Y, Kohama I, and Aoki M.** Afferent projections to the Botzinger complex from the upper cervical cord and other respiratory related structures in the brainstem in cats: retrograde WGA-HRP tracing. *J Auton Nerv Syst* 56: 1-7, 1995.
- Geerling JC, Yokota S, Rukhadze I, Roe D, and Chamberlin NL.** Kolliker-Fuse GABAergic and glutamatergic neurons project to distinct targets. *J Comp Neurol* 525: 1844-1860, 2017.

Guthmann A, Fritschy JM, Ottersen OP, Torp R, and Herbert H. GABA, GABA transporters, GABA(A) receptor subunits, and GAD mRNAs in the rat parabrachial and Kolliker-Fuse nuclei. *J Comp Neurol* 400: 229-243, 1998.

Harris MB, and Milsom WK. Apneusis follows disruption of NMDA-type glutamate receptors in vagotomized ground squirrels. *Respir Physiol Neurobiol* 134: 191-207, 2003.

Iizuka M, and Fregosi RF. Influence of hypercapnic acidosis and hypoxia on abdominal expiratory nerve activity in the rat. *Respir Physiol Neurobiol* 157: 196-205, 2007.

Janczewski WA, and Feldman JL. Distinct rhythm generators for inspiration and expiration in the juvenile rat. *J Physiol* 570: 407-420, 2006.

Jenkin SE, and Milsom WK. Expiration: breathing's other face. *Prog Brain Res* 212: 131-147, 2014.

Jenkin SE, Milsom WK, and Zoccal DB. The Kolliker-Fuse Nucleus acts as a timekeeper for late-expiratory abdominal activity. *Neuroscience* 2017.

Leirao IP, Silva CA, Jr., Gargaglioni LH, and da Silva GSF. Hypercapnia-induced active expiration increases in sleep and enhances ventilation in unanaesthetized rats. *J Physiol* 2017.

Lemes EV, and Zoccal DB. Vagal afferent control of abdominal expiratory activity in response to hypoxia and hypercapnia in rats. *Respir Physiol Neurobiol* 203: 90-97, 2014.

Levitt ES, Abdala AP, Paton JF, Bissonnette JM, and Williams JT.  $\mu$  opioid receptor activation hyperpolarizes respiratory-controlling Kolliker-Fuse neurons and suppresses post-inspiratory drive. *J Physiol* 593: 4453-4469, 2015.

Lumsden T. Observations on the respiratory centres in the cat. *J Physiol* 57: 153-160, 1923.

Mandel DA, and Schreihöfer AM. Modulation of the sympathetic response to acute hypoxia by the caudal ventrolateral medulla in rats. *J Physiol* 587: 461-475, 2009.

Marina N, Abdala AP, Trapp S, Li A, Nattie EE, Hewinson J, Smith JC, Paton JF, and Gourine AV. Essential role of Phox2b-expressing ventrolateral brainstem neurons in the chemosensory control of inspiration and expiration. *J Neurosci* 30: 12466-12473, 2010.

McCormick DA, and Pape HC. Properties of a hyperpolarization-activated cation current and its role in rhythmic oscillation in thalamic relay neurones. *J Physiol* 431: 291-318, 1990.

Mifflin SW. Arterial chemoreceptor input to respiratory hypoglossal motoneurons. *J Appl Physiol* (1985) 69: 700-709, 1990.

Molkov YI, Abdala AP, Bacak BJ, Smith JC, Paton JF, and Rybak IA. Late-expiratory activity: emergence and interactions with the respiratory CpG. *J Neurophysiol* 104: 2713-2729, 2010.

Molkov YI, Bacak BJ, Dick TE, and Rybak IA. Control of breathing by interacting pontine and pulmonary feedback loops. *Frontiers in neural circuits* 7: 16, 2013.

Molkov YI, Shevtsova NA, Park C, Ben-Tal A, Smith JC, Rubin JE, and Rybak IA. A closed-loop model of the respiratory system: focus on hypercapnia and active expiration. *PLoS one* 9: e109894, 2014.

Molkov YI, Zoccal DB, Moraes DJ, Paton JF, Machado BH, and Rybak IA. Intermittent hypoxia-induced sensitization of central chemoreceptors contributes to sympathetic nerve activity during late expiration in rats. *J Neurophysiol* 105: 3080-3091, 2011a.

Molkov YI, Zoccal DB, Moraes DJ, Paton JF, Machado BH, and Rybak IA. Intermittent hypoxia-induced sensitization of central chemoreceptors contributes to sympathetic nerve activity during late expiration in rats. *J Neurophysiol* 105: 3080-3091, 2011b.



**Moraes DJ, Bonagamba LG, Costa KM, Costa-Silva JH, Zoccal DB, and Machado BH.** Short-term sustained hypoxia induces changes in the coupling of sympathetic and respiratory activities in rats. *The Journal of physiology* 592: 2013-2033, 2014.

**Moraes DJ, da Silva MP, Bonagamba LG, Mecawi AS, Zoccal DB, Antunes-Rodrigues J, Varanda WA, and Machado BH.** Electrophysiological properties of rostral ventrolateral medulla presympathetic neurons modulated by the respiratory network in rats. *J Neurosci* 33: 19223-19237, 2013.

**Moraes DJ, Dias MB, Cavalcanti-Kwiatkoski R, Machado BH, and Zoccal DB.** Contribution of retrotrapezoid/parafacial respiratory region to the expiratory-sympathetic coupling in response to peripheral chemoreflex in rats. *J Neurophysiol* 108: 882-890, 2012.

**Moreira TS, Takakura AC, Colombari E, West GH, and Guyenet PG.** Inhibitory input from slowly adapting lung stretch receptors to retrotrapezoid nucleus chemoreceptors. *J Physiol* 580: 285-300, 2007.

**Morrison SF, Cravo SL, and Wilfehrt HM.** Pontine lesions produce apneusis in the rat. *Brain Res* 652: 83-86, 1994.

**Morschel M, and Dutschmann M.** Pontine respiratory activity involved in inspiratory/expiratory phase transition. *Philosophical transactions of the Royal Society of London Series B, Biological sciences* 364: 2517-2526, 2009.

**Orem J, and Trotter RH.** Postinspiratory neuronal activities during behavioral control, sleep, and wakefulness. *J Appl Physiol* (1985) 72: 2369-2377, 1992.

**Pagliardini S, Janczewski WA, Tan W, Dickson CT, Deisseroth K, and Feldman JL.** Active expiration induced by excitation of ventral medulla in adult anesthetized rats. *J Neurosci* 31: 2895-2905, 2011.

**Paton JF.** The ventral medullary respiratory network of the mature mouse studied in a working heart-brainstem preparation. *J Physiol* 493 ( Pt 3): 819-831, 1996.

**Paxinos G, and Watson C.** *The rat brain in stereotaxic coordinates*. Amsterdam ; Boston :: Academic Press/Elsevier, 2007.

**Rosin DL, Chang DA, and Guyenet PG.** Afferent and efferent connections of the rat retrotrapezoid nucleus. *J Comp Neurol* 499: 64-89, 2006.

**Rubin JE, Bacak BJ, Molkov YI, Shevtsova NA, Smith JC, and Rybak IA.** Interacting oscillations in neural control of breathing: modeling and qualitative analysis. *J Comput Neurosci* 30: 607-632, 2011.

**Rybak IA, Abdala AP, Markin SN, Paton JF, and Smith JC.** Spatial organization and state-dependent mechanisms for respiratory rhythm and pattern generation. *Prog Brain Res* 165: 201-220, 2007.

**Rybak IA, Paton JF, and Schwaber JS.** Modeling neural mechanisms for genesis of respiratory rhythm and pattern. I. Models of respiratory neurons. *J Neurophysiol* 77: 1994-2006, 1997.

**Rybak IA, Shevtsova NA, Paton JF, Dick TE, St-John WM, Morschel M, and Dutschmann M.** Modeling the ponto-medullary respiratory network. *Respir Physiol Neurobiol* 143: 307-319, 2004.

**Silva JN, Lucena EV, Silva TM, Damasceno RS, Takakura AC, and Moreira TS.** Inhibition of the pontine Kolliker-Fuse nucleus reduces genioglossal activity elicited by stimulation of the retrotrapezoid chemoreceptor neurons. *Neuroscience* 328: 9-21, 2016a.

**Silva JN, Tanabe FM, Moreira TS, and Takakura AC.** Neuroanatomical and physiological evidence that the retrotrapezoid nucleus/parafacial region regulates expiration in adult rats. *Respir Physiol Neurobiol* 227: 9-22, 2016b.

**Smith JC, Abdala AP, Koizumi H, Rybak IA, and Paton JF.** Spatial and functional architecture of the mammalian brain stem respiratory network: a hierarchy of three oscillatory mechanisms. *J Neurophysiol* 98: 3370-3387, 2007.

**Smith JC, Ellenberger HH, Ballanyi K, Richter DW, and Feldman JL.** Pre-Botzinger complex: a brainstem region that may generate respiratory rhythm in mammals. *Science* 254: 726-729, 1991.

**St-John WM, and Paton JF.** Role of pontile mechanisms in the neurogenesis of eupnea. *Respir Physiol Neurobiol* 143: 321-332, 2004.

**Takakura AC, Moreira TS, West GH, Gwilt JM, Colombari E, Stornetta RL, and Guyenet PG.** GABAergic Pump Cells of Solitary Tract Nucleus Innervate Retrotrapezoid Nucleus Chemoreceptors. *J Neurophysiol* 98: 374-381, 2007.

**Teppema LJ, Veening JG, Kranenburg A, Dahan A, Berkenbosch A, and Olivier C.** Expression of c-fos in the rat brainstem after exposure to hypoxia and to normoxic and hyperoxic hypercapnia. *J Comp Neurol* 388: 169-190, 1997.

**Toward MA, Abdala AP, Knopp SJ, Paton JF, and Bissonnette JM.** Increasing brain serotonin corrects CO<sub>2</sub> chemosensitivity in methyl-CpG-binding protein 2 (Mecp2)-deficient mice. *Exp Physiol* 98: 842-849, 2013.

**Yokota S, Kaur S, VanderHorst VG, Saper CB, and Chamberlin NL.** Respiratory-related outputs of glutamatergic, hypercapnia-responsive parabrachial neurons in mice. *J Comp Neurol* 523: 907-920, 2015.

**Zoccal DB, Bonagamba LG, Paton JF, and Machado BH.** Sympathetic-mediated hypertension of awake juvenile rats submitted to chronic intermittent hypoxia is not linked to baroreflex dysfunction. *Exp Physiol* 94: 972-983, 2009.

**Zoccal DB, Simms AE, Bonagamba LG, Braga VA, Pickering AE, Paton JF, and Machado BH.** Increased sympathetic outflow in juvenile rats submitted to chronic intermittent hypoxia correlates with enhanced expiratory activity. *J Physiol* 586: 3253-3265, 2008.

## TABLES

**Table 1.** Detailed connectivity of the computational model.

Target Population	Excitatory drive [weight of synaptic input] or presynaptic source population [weight of synaptic input from single neuron]
aug-E (BotC)	Drive (PONS) [0.42] <sup>a</sup> , Drive (RTN) [2.3] <sup>b</sup> , early-I (1) (pre-BötC) [-0.135], late-E (pFRG) [0.03] <sup>b</sup> , post-I (BötC) [-0.3]
early-I (1) (pre-BotC)	Drive (RTN) [2] <sup>a</sup> , Drive (KF) [0.6] <sup>bd</sup> , aug-E (BötC) [-0.265], post-I (BötC) [-0.45], pre-I (pre-BötC) [0.05] <sup>a</sup>
early-I (2) (rVRG)	Drive (PONS) [2.5], aug-E (BötC) [-0.25], post-I (BötC) [-0.5]
late-E (pFRG)	Drive (RTN) [0.225, 0.325] <sup>ac</sup> , early-I (1) (pre-BötC) [-0.05] <sup>a</sup> , late-E (pFRG) [0.024] <sup>a</sup> , post-I (BötC) [-0.0275] <sup>a</sup> , pre-I (pre-BötC) [0.013] <sup>b</sup>
post-I (BotC)	Drive (PONS) [1] <sup>a</sup> , Drive (KF) [0.65] <sup>bd</sup> , early-I (1) (pre-BötC) [-0.025]
post-I (e) (BotC)	Drive (PONS) [0.8] <sup>a</sup> , aug-E (BötC) [-0.3] <sup>a</sup> , early-I (1) (pre-BötC) [-0.2] <sup>a</sup>
pre-I (pre-BotC)	Drive (RTN) [0.198, 0.286] <sup>c</sup> , Drive (PONS) [0.65], Drive (Raphe) [0.15] <sup>a</sup> , aug-E (BötC) [-0.01] <sup>a</sup> , post-I (BötC) [-0.19] <sup>a</sup> , pre-I (pre-BötC) [0.02] <sup>a</sup>
ramp-I (rVRG)	Drive (PONS) [2], aug-E (BötC) [-0.1], early-I (2) (rVRG) [-0.3], post-I (BötC) [-2], pre-I (pre-BötC) [0.12]
	<sup>a</sup> Different value from Molkov et al. (2011b) <sup>b</sup> Not Present in Molkov et al. (2011b) <sup>c</sup> Drive (RTN) [Eucapnia, Hypercapnia] <sup>d</sup> Isoguvacine and Gabazine

## FIGURE LEGENDS

**Figure 1. Functional and histological identification of the Kölliker-Fuse.** **A:** Integrated recordings of abdominal (AbN), phrenic (PN) and cervical vagus (cVN) nerve activities from an *in situ* rat preparation, representative of the group, illustrating the respiratory responses to microinjections of glutamate (arrow) in the left (top) and right sides (bottom) of Kölliker-Fuse (KF). \* represents an artifact generated during the removal of the injection micropipette. **B:** Photomicrography of coronal section from the brainstem of a representative *in situ* rat preparation, illustrating the site of microinjection in the KF (arrow). **C:** Schematic representations of all microinjection sites (black circles) into the KF (n = 6 each side). Abbreviation: DLL – dorsal nucleus of the lateral lemniscus; scp: superior cerebellar peduncle; s5 – sensory root of trigeminal nerve; 4V – fourth ventricle.

**Figure 2. Changes in baseline activities after microinjections of gabazine in the Kölliker-Fuse.** **A:** Raw and integrated recordings of cervical vagus (cVN), phrenic (PN) and abdominal nerve activities (AbN) from a representative *in situ* rat preparation, illustrating the respiratory pattern before and after gabazine microinjections in the Kölliker-Fuse (KF). **B-E:** Average values of cVN post-I duration (normalized by expiratory time), coefficient of variation of PN burst frequency, mean PN burst frequency and mean abdominal activity, respectively, before and after gabazine microinjections in the KF. \* - different from baseline,  $P < 0.05$ ,  $n = 6$ .

**Figure 3. Disinhibition of the Kölliker-Fuse suppresses the generation of abdominal late-E activity during hypercapnia.** Recordings, from representative *in situ* rat preparations, depict the activity of central vagus nerve (cVN), phrenic nerve (PN), and abdominal nerve (AbN) in eucapnia and hypercapnia, pre-treatment (**A-E**) and after gabazine microinjections (**F-J**). All recordings performed after gabazine microinjections are indicated in the light grey box. Filled arrows and unfilled arrows in panels A and F indicate the beginning and end of the change in perfusate CO<sub>2</sub> fractional concentration from 5% to 8%, respectively. Zoomed in traces, **B, D, G and I** depict respective preceding eucapnia epochs; **C and H** depict 8% hypercapnia; and **E and J** depict 10% hypercapnia. Traces **A-C** and **F-H** are from a preparation challenged with 8% CO<sub>2</sub>. Traces **D, E, I and J** come from a separate preparation which was challenged with 10% CO<sub>2</sub>.

**Figure 4. Disinhibition of the Kölliker-Fuse prevented the reduction in vagal post-inspiratory activity and restrained the generation of late-E abdominal activity during hypercapnia. A-B:** Superimposed traces of integrated cervical vagus (cVN, gray) and abdominal nerve activities (AbN, black) during hypercapnia, from a representative *in situ* rat preparation, before and after gabazine microinjections in the Kölliker-Fuse (KF). The gray box indicates the inspiratory phase (coincident with phrenic burst) and the arrows indicate the end of post-inspiratory (post-I) activity in cVN. Note that before gabazine microinjections, the onset of the late-E burst in AbN during hypercapnia is associated with a clear truncation in post-I activity. After gabazine microinjections, the amplitude of AbN late-E burst reduced and post-I cVN activity presented minor changes. **C-D:** Average values of AbN late-E burst amplitude and variation of cVN post-I duration during hypercapnia, before and after gabazine microinjections in the KF. \* statistically significantly different from baseline,  $P < 0.05$ ,  $n = 6$ .

**Figure 5. Schematic of the brainstem respiratory network model** including the inhibitory post-inspiratory (post-I), excitatory post-inspiratory (post-I(e)), and augmenting expiratory (aug-E) populations of the Bötzinger complex (BötC); the pre-inspiratory/inspiratory (pre-I/I) and early-inspiratory (early-I (1)) populations of the pre-Bötzinger complex (pre-BötC); the ramping inspiratory (ramp-I) and early-inspiratory [early-I (2)] populations of the rostral ventral respiratory group (rVRG); and the late-expiratory (late-E) population of the parafacial respiratory group (pFRG). This model includes excitatory drive elements, which are not modeled as populations and provide constant excitation to post-synaptic populations: drive from the pontine nuclei (Drive Pons), drive specifically from the Kölliker-Fuse (Drive KF), and drive from the retrotrapezoid nucleus (Drive RTN). Excitatory and inhibitory populations of 20 to 50 neurons are respectively depicted as orange and blue elements. Similarly, projections from excitatory and inhibitory populations are respectively colored orange and blue. Drive elements and projections associated with these elements are represented as green triangles or green arrows. The new additions to this model—Drive KF and its projections—are emphasized with black outline.

**Figure 6. Simulation of the glutamate microinjection into the Kölliker-Fuse** by transient increase in drive from the Kölliker-Fuse to the respiratory CPG (arrow). The figure shows the activity of the phrenic nerve (PN) and the central vagus nerve (cVN) as well as the inhibitory post-inspiratory (post-I), excitatory post-inspiratory (post-I (e)), and augmenting-expiratory (aug-E) populations of the Bötzing complex (BötC).

**Figure 7. Simulation of the Kölliker-Fuse inhibition in eucapnia.** Model activity of central pattern generator populations under (A) eucapnia and (B) KF inhibition. The figure shows the activities of the pre-inspiratory/inspiratory (pre-I/I) population of the pre-Bötzing complex (pre-BötC); the inhibitory post-inspiratory (post-I), augmenting expiratory (aug-E), and excitatory post-inspiratory (post-I (e)) populations of the Bötzing complex (BötC); and the late-expiratory (late-E) population of the pFRG. The horizontal black line emphasizes the change in amplitude of the inhibitory post-I population between (A) and (B).

**Figure 8. Simulation of the Kölliker-Fuse inhibition and disinhibition in hypercapnia.** Motoneuron output in the model under (A) hypercapnia plus KF inhibition, (B) hypercapnia, and (C) hypercapnia plus KF excitation each depicting activity of the phrenic nerve (PN), the central vagus nerve (cVN), and the abdominal nerve (AbN).

**Figure 9. Simulation of the Kölliker-Fuse inhibition and disinhibition in hypercapnia.** Model activity of central pattern generator populations under (A) hypercapnia plus KF inhibition, (B) hypercapnia, and (C) hypercapnia plus KF excitation. The post-I (BötC) traces are shaded grey for emphasis. The horizontal dashed black line in the post-I (BötC) traces indicate the approximate threshold for activation of the late-E (pFRG). The vertical dashed grey lines indicate the phase of activation of late-E (pFRG). The included populations are the pre-inspiratory/inspiratory (pre-I/I) population of the pre-Bötzing complex (pre-BötC); the inhibitory post-inspiratory (post-I), augmenting expiratory (aug-E), and excitatory post-inspiratory (post-I (e)) populations of the Bötzing complex (BötC); and the late-expiratory (late-E) population of the pFRG.

893 **Figure 10. Comparison of post-inspiratory activity among three hypercapnia simulations.**  
894 Activity of the post-I (e) (BötC) determines the post-inspiratory component of the cVN burst.  
895 The vertical grey line in each trace indicates the end of the post-inspiratory burst.

# FIGURES

Figure 1

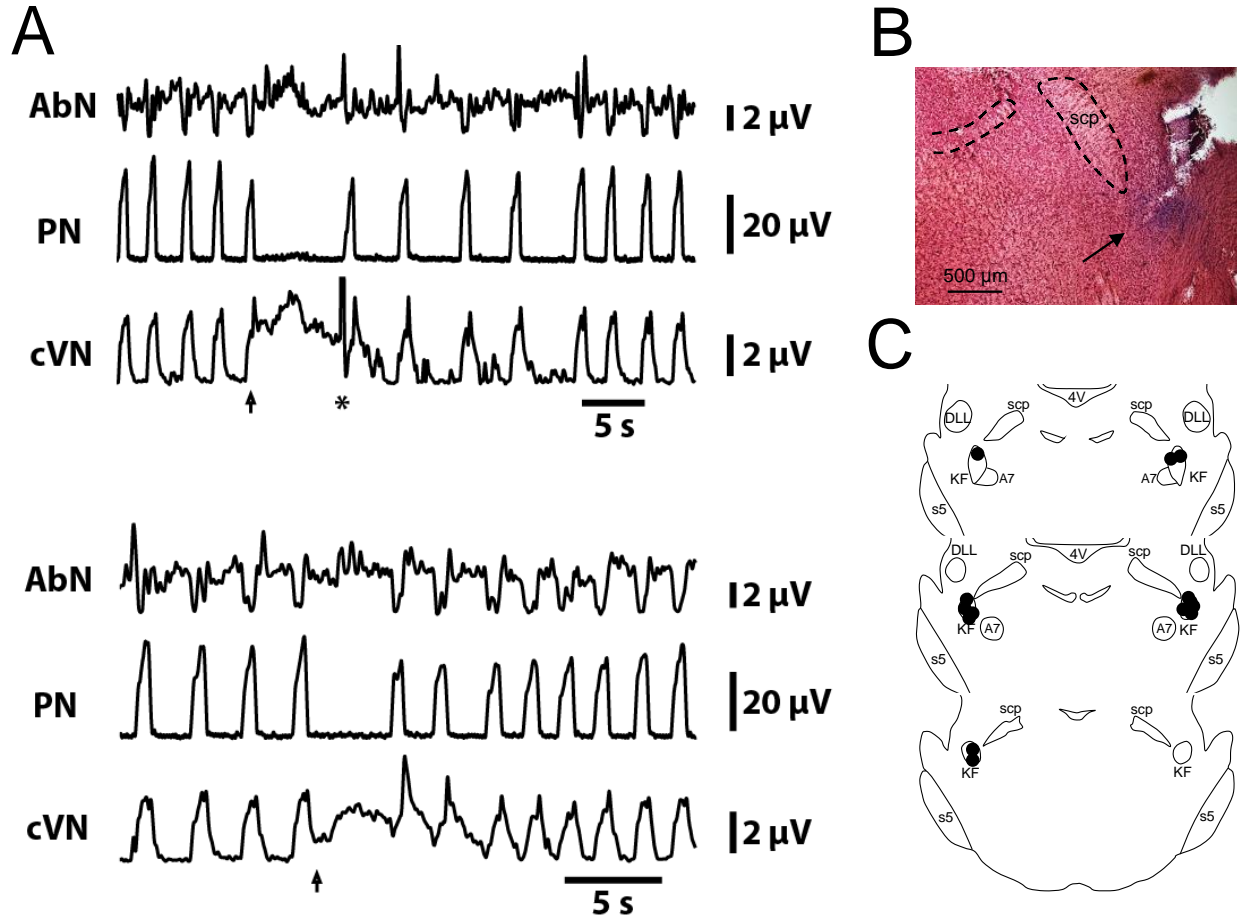
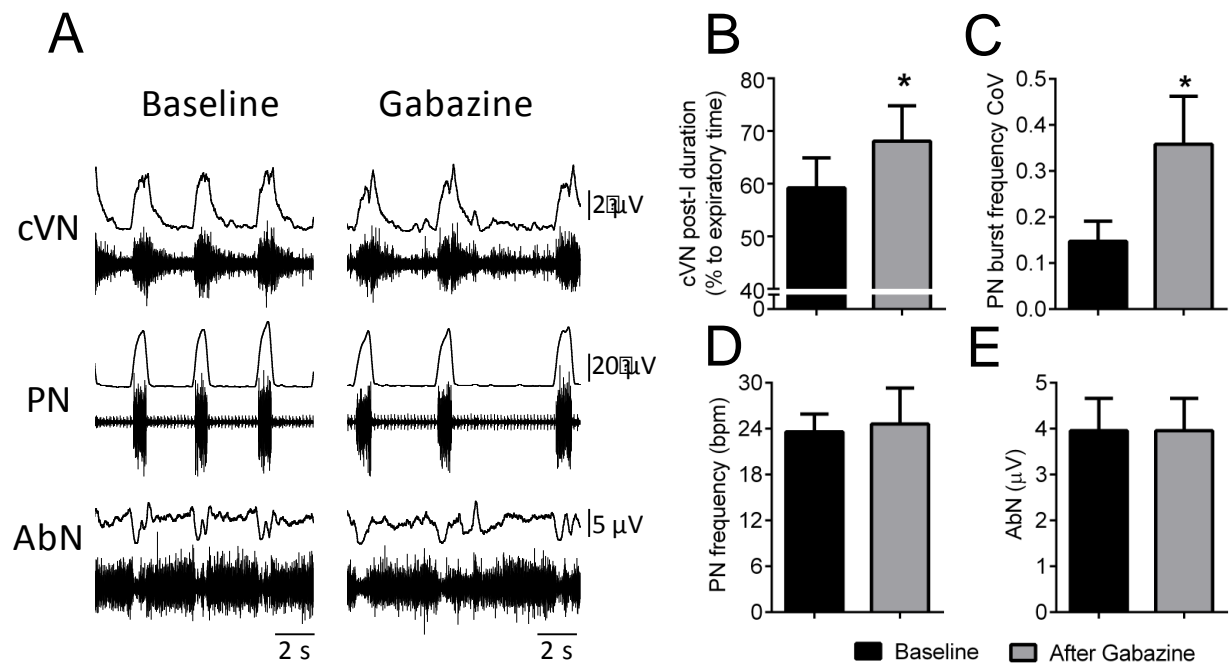
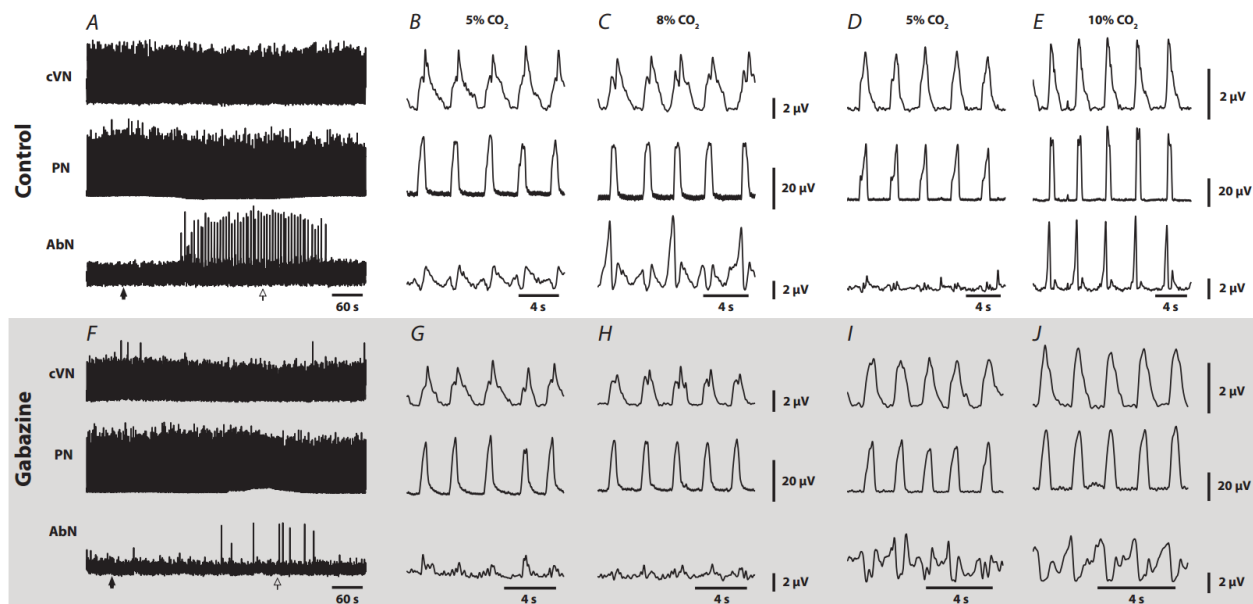




Figure 2



**Figure 3**



**Figure 4**

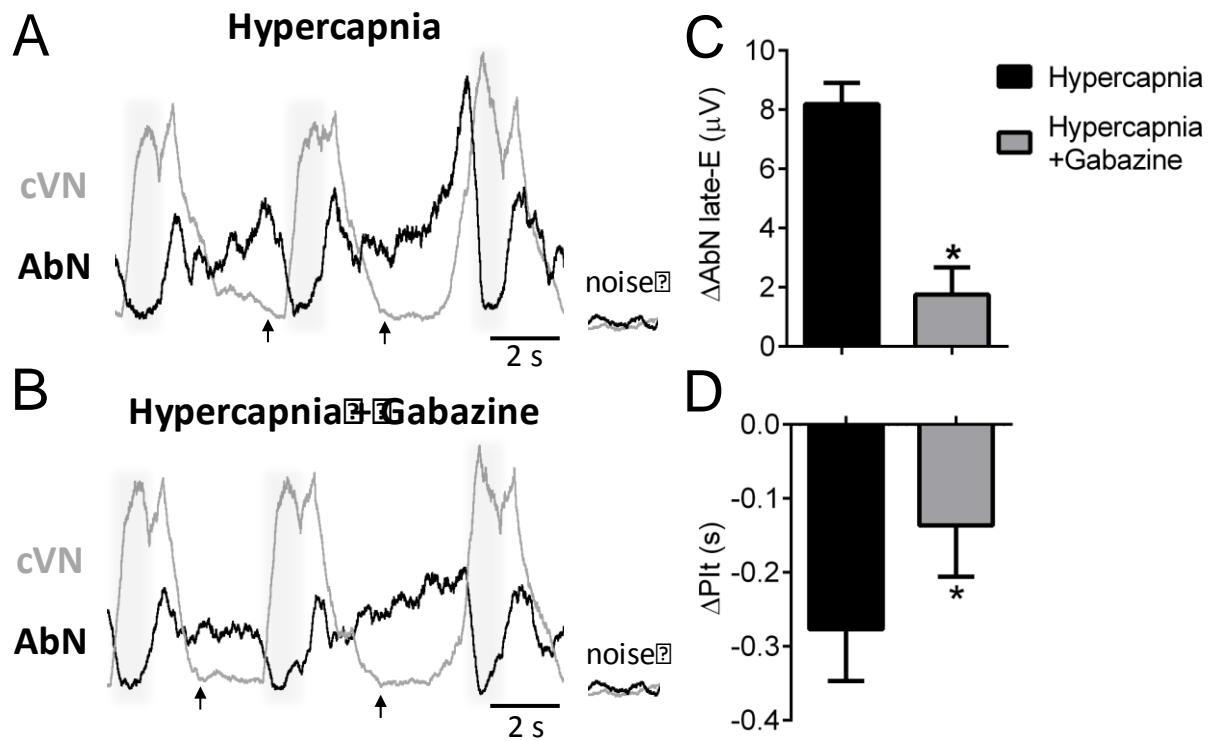
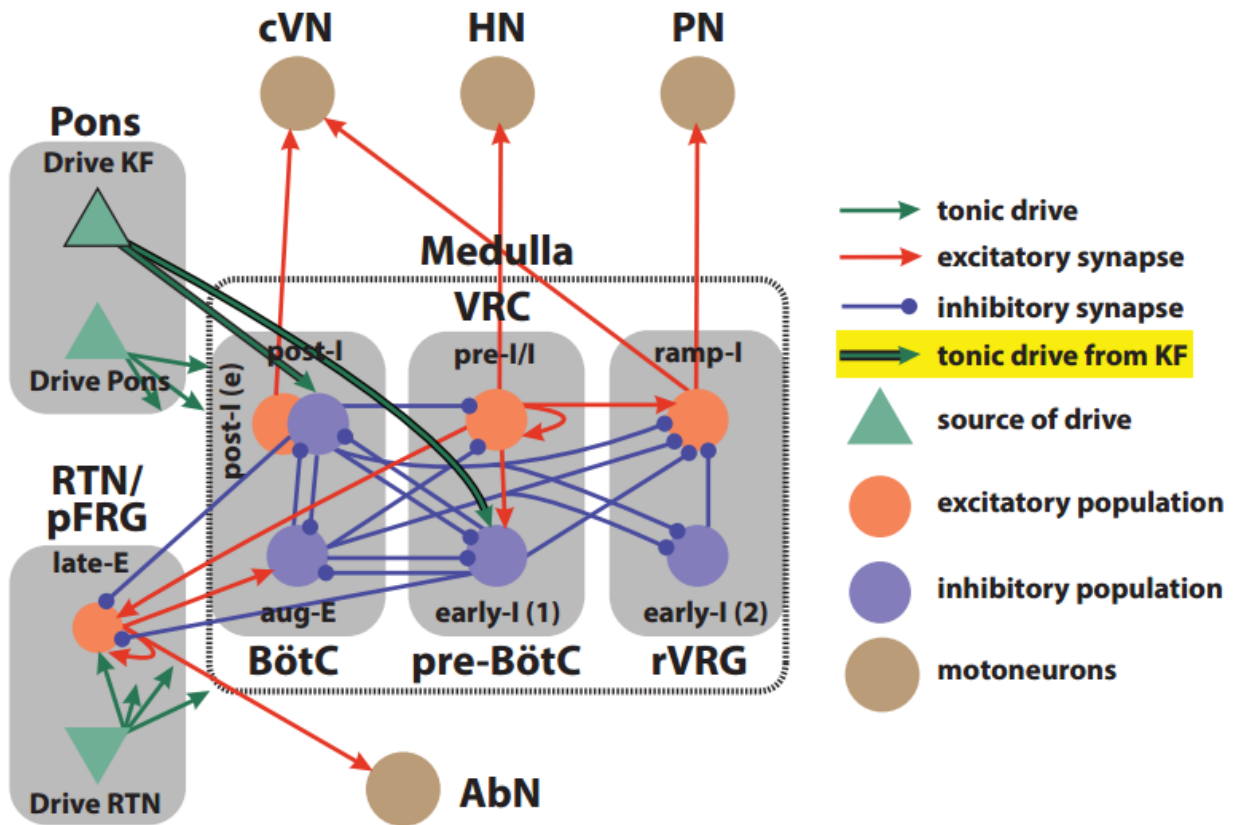


Figure 5



**Figure 6**



**Figure 7**

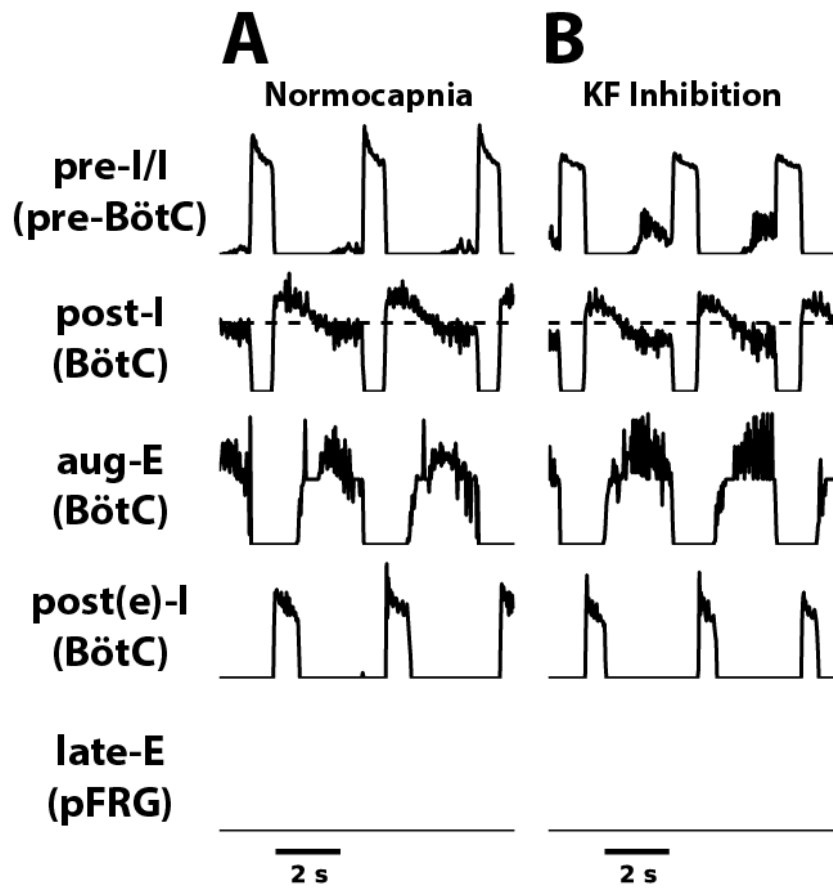


Figure 8

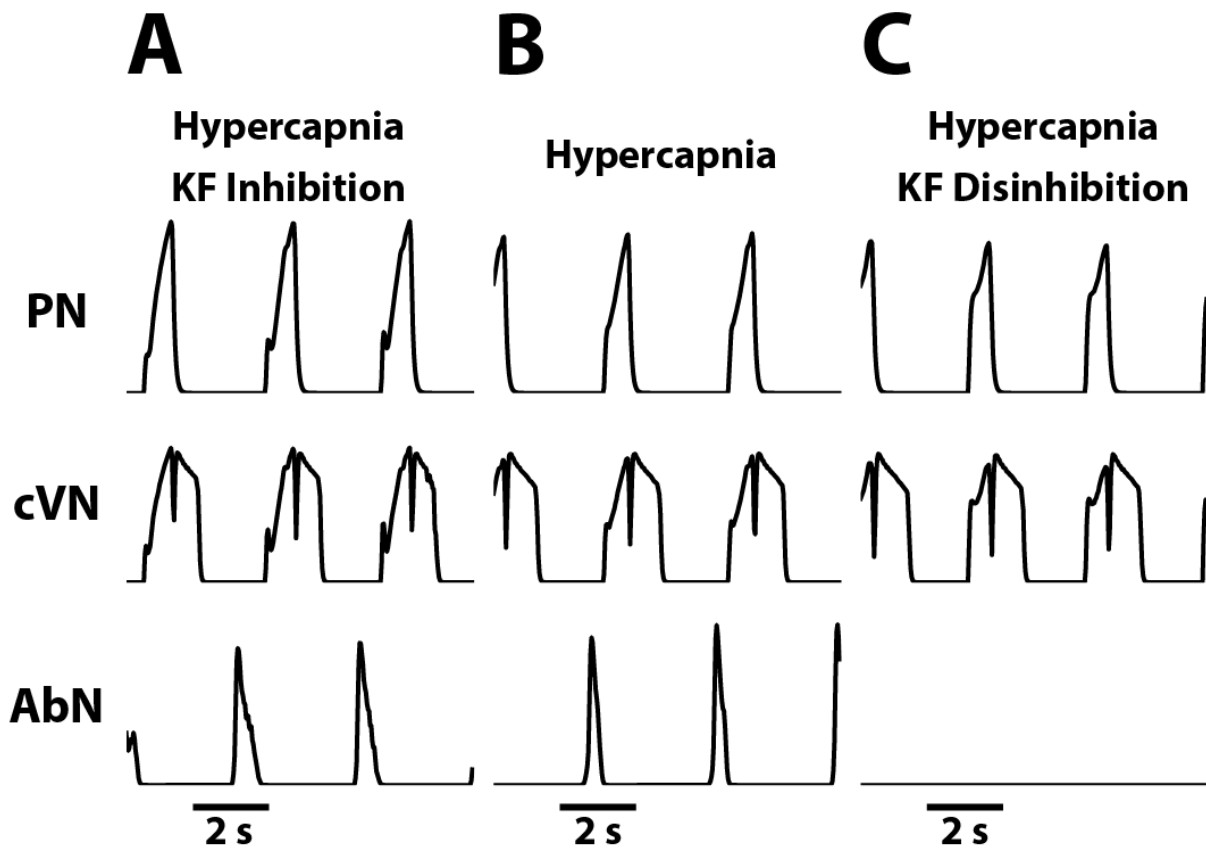
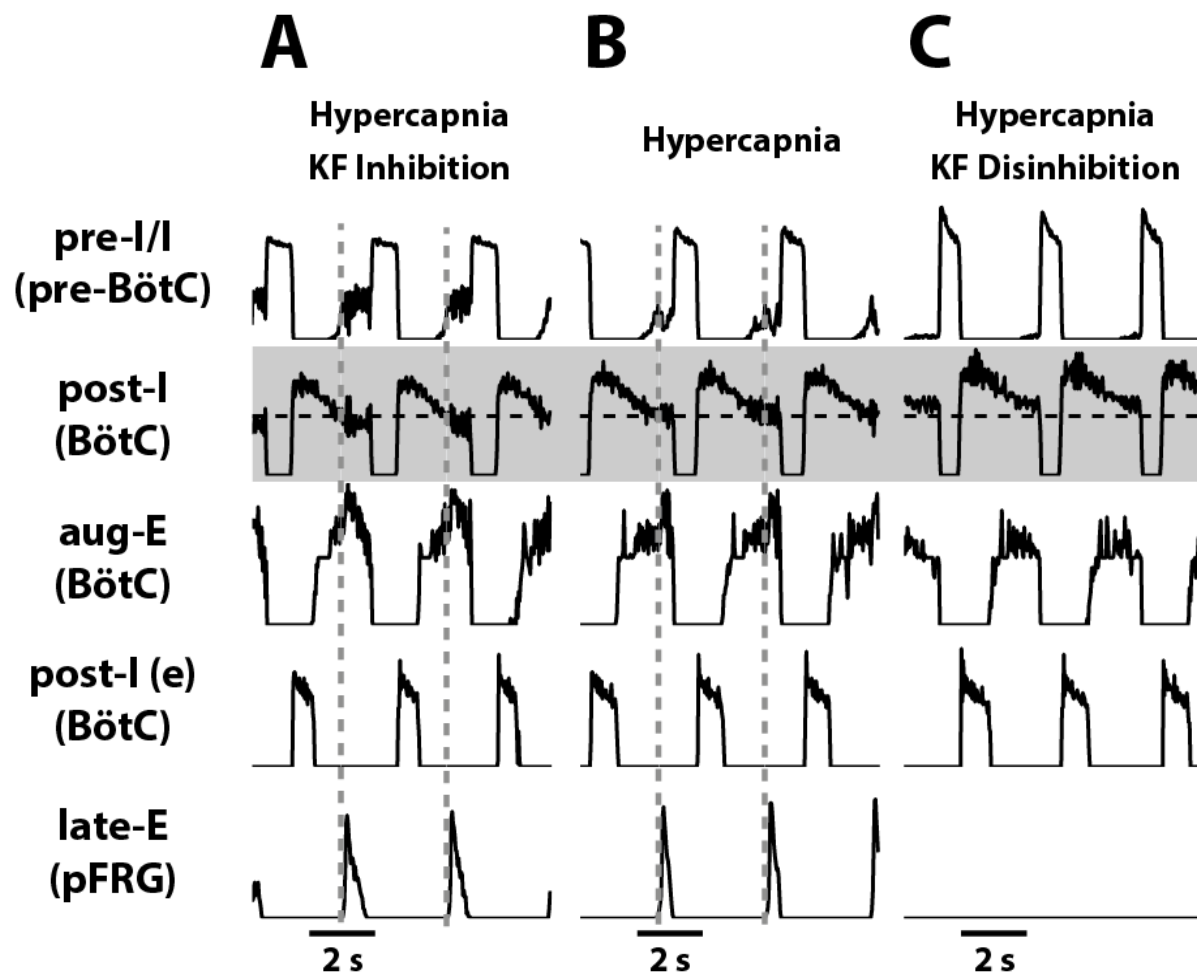


Figure 9





1198  
1199  
1200  
1201

**Figure 10**

